Journal of Solid State Chemistry 186 (2012) 195–203

Contents lists available at SciVerse ScienceDirect

Journal of Solid State Chemistry

journal homepage: www.elsevier.com/locate/jssc

Low temperature fluorination of $Sr_3Fe_2O_{7-x}$ with polyvinylidine fluoride: An X-ray powder diffraction and Mössbauer spectroscopy study

Cathryn A. Hancock [a], Tirma Herranz [b], Jose F. Marco [b], Frank J. Berry [a], Peter R. Slater [a,*]

[a] School of Chemistry, The University of Birmingham, Edgbaston, Birmingham B15 2TT, UK
[b] Instituto de Quimica Fisica, Consejo Superior de Investigaciones Cientificas, Seranno 119, 28006 Madrid, Spain

ARTICLE INFO

Article history:
Received 13 September 2011
Received in revised form
8 December 2011
Accepted 11 December 2011
Available online 16 December 2011

Keywords:
Ruddlesden Popper phase
Fluorination
Mössbauer spectroscopy

ABSTRACT

Fluorination of the Ruddlesden Popper phase, $Sr_3Fe_2O_{7-x}$ by heat treatment with polyvinylidine fluoride (PVDF) gives a range of novel oxide fluoride compounds. Fluorination with 1 mol equivalent PVDF leads to a filling of the normal Ruddlesden Popper structure anion sites and a material of composition $Sr_3Fe_2O_{5+x}F_{2-x}$ ($x \approx 0.28(4)$) which contains both Fe^{4+} and Fe^{3+}. Increasing the amount of PVDF to 2 mol equivalent leads to an increase in anion content due to filling of half the interstitial sites within the structure, with iron being completely reduced to Fe^{3+} leading to a composition $Sr_3Fe_2O_4F_4$. An increase in the amount of PVDF to ≈ 3 mol equivalent leads to a further increase in unit cell volume, attributed to complete filling of the interstitial sites and a composition $Sr_3Fe_2O_3F_6$. ^{57}Fe Mössbauer spectra in the temperature range 10–300 K demonstrated the complexity of the magnetic interactions in each of the three phases which reflect different local compositions of oxygen and fluorine around the iron ions thus influencing the superexchange pathways.

1. Introduction

Perovskite-related materials have attracted substantial interest due to the wide range of important properties displayed by materials with this structure-type. Most of this research has been focused on simple oxide systems, although the synthesis of mixed oxide fluorides offers avenues to new materials with interesting properties. However, such oxide fluoride materials generally require alternative low temperature synthesis routes due to the high thermodynamic stability of simple binary fluorides, such as alkaline earth fluorides, although recently there have been reports of improved stability in hexagonal perovskites with low fluorine contents [1,2]. Much of the work in this area has focused on copper-containing systems following the identification of superconductivity in oxide fluorides of composition $Sr_2CuO_2F_{2+x}$ [3–5]. Recently we have been extending this fluorination work to perovskite-related materials containing other transition metals. In particular we have investigated the fluorination of oxygen deficient $AFeO_{3-\delta}$ (A=Sr, Ba) [6–10]. This work made use of a new fluorination reagent, polyvinylidine fluoride (PVDF); the use of fluorine-containing polymers offers a more flexible control of the fluorine content than fluorination by other techniques, e.g. heating in fluorine gas [11–14]. In addition, contrary to reaction with F_2 gas, which is highly oxidizing, the reaction with PVDF is nonoxidizing and indeed our prior work on oxygen deficient $AFeO_{3-\delta}$ (A=Sr, Ba) showed that PVDF reduced the Fe oxidation state to Fe^{3+} [6–10]. In terms of perovskite-related Fe containing systems, the Ruddlesden Popper phase $Sr_3Fe_2O_{7-x}$ has attracted significant interest. Ruddlesden Popper phases have general formula $A_{n+1}M_nO_{3n+1}$ (A=alkaline earth, rare earth, M=transition metals, Ga, Al, etc.), and their structures may be viewed as an intergrowth between perovskite and rock salt units. $Sr_3Fe_2O_{7-x}$ is therefore an n=2 Ruddlesden Popper phase (structure shown in Fig. 1), where complete filling of the ideal oxygen anion sites within the perovskite and rock salt layers would lead to a total oxygen content of 7.0 (in the rest of the paper these will be referred to as the normal anion sites). An interesting additional aspect of these Ruddlesden Popper phases is that they also have the possibility of the incorporation of anions into interstitial sites; these anions occupy fluorite-type positions within the rock salt layers (in the rest of the paper these will be referred to as interstitial anion sites).

$Sr_3Fe_2O_{7-x}$ has been previously examined in detail by a number of researchers. This system might nominally be expected to contain mixed valence Fe^{3+}/Fe^{4+}; however, ^{57}Fe Mössbauer spectroscopy has suggested the disproportionation of Fe^{4+} into Fe^{3+} and Fe^{5+} [15–20]. Fluorination of this system has also been examined by Weller and co-workers who first reduced $Sr_3Fe_2O_{7-x}$ to $Sr_3Fe_2O_6$ before performing oxidation with F_2 gas to give $Sr_3Fe_2O_6F_{0.87}$ [21]. ^{57}Fe Mössbauer spectra indicated that, as for

* Corresponding author. Fax: +44 1483 686851.
E-mail address: p.r.slater@bham.ac.uk (P.R. Slater).

0022-4596/$ - see front matter © 2011 Elsevier Inc. All rights reserved.
doi:10.1016/j.jssc.2011.12.016

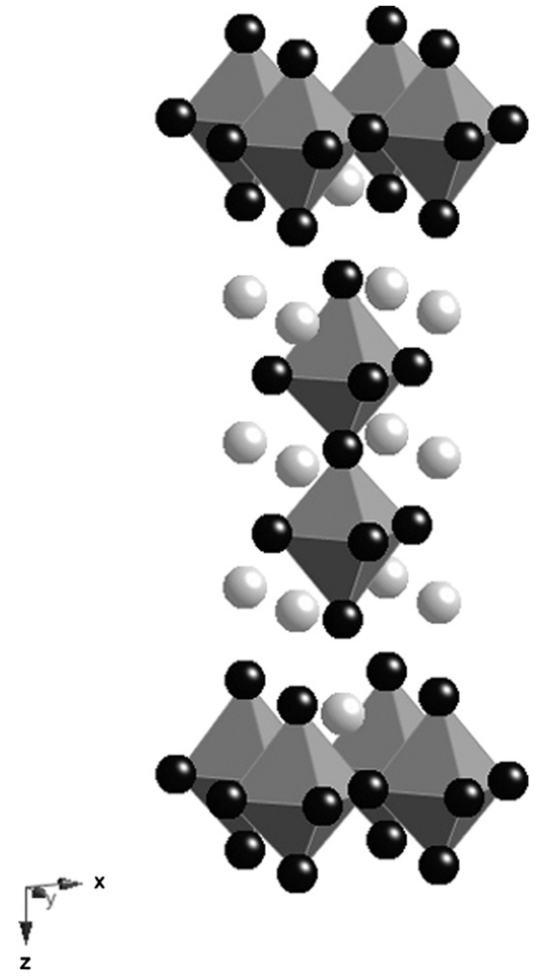

Fig. 1. Structure of $Sr_3Fe_2O_{7-x}$ (Sr=light gray spheres, O=black spheres, Fe at the center of the octahedra).

the simple oxide, the Fe was present in 3+ and 5+ oxidation states. Recently, Tsujimoto et al.[22] have reported higher fluorine contents by fluorination using polytetrafluoroethylene (PTFE), leading to a composition $Sr_3Fe_2O_{5.44}F_{1.56}$, with all the normal anion sites filled, and no occupancy of the interstitial anion sites.

In this work we examine the fluorination of $Sr_3Fe_2O_{7-x}$ with PVDF and show that this route can lead to far higher fluorine contents. In particular incorporation of fluorine into interstitial sites within the rock salt layers is shown to occur for samples with high fluorine contents. The samples have been characterized by X-ray powder diffraction and ^{57}Fe Mössbauer spectroscopy.

2. Experimental details

$Sr_3Fe_2O_{7-x}$ was prepared by the calcination of appropriate quantities of a well ground mixture of $SrCO_3$ and Fe_2O_3 at 1100 °C for 24 h in air with intermediate regrinding. The oxygen content of this phase was determined from thermogravimetric analysis (TGA) experiments (Netzsch STA 449 F1 Jupiter Thermal Analyzer). The material was heated at 10 °C/min to 1200 °C in N_2 and held for 30 min to reduce the transition metal oxidation state to 3+, with the original oxygen content then being determined from the mass loss observed.

Fluorination was achieved by mixing the $Sr_3Fe_2O_{7-x}$ phase with poly(vinylidene fluoride) (PVDF) in 1:1, 1:2 and 1:3 mol ratios (precursor oxide:CH_2CF_2 monomer unit) and heating this mixture at 375 °C for 24 h in air in a furnace within a fume cupboard with an intermediate regrind. The ratios were chosen with the intention of producing phases containing 2, 4, and 6F per formula unit respectively (a small 5% excess of PVDF was added in each case to overcome potential loss before reaction). The fluorination process can be classed as a type of metathesis reaction, where the F from the polymer replaces O in the sample, with the reaction being performed in air helping to ensure burn off of any residual C from the polymer. The exchange could either result in no change in Fe oxidation state (2F in place of 1O) or lead to partial reduction (1F in place of 1O). In practice a mixture of the two processes tends to occur as shown in fluorination of related iron containing systems [7–10,22].

X-ray powder diffraction patterns were recorded with a Bruker D8 diffractometer using Cu$K\alpha$ radiation at 298 K. The X-ray diffraction data provided an indication of the purity of the samples and was also used for structural characterization. For the latter, Rietveld refinement of the X-ray powder diffraction data used the GSAS suite of programs [23].

The ^{57}Fe Mössbauer spectra were recorded in constant acceleration mode using a *ca.* 25 mCi ^{57}Co/Rh source and a helium closed-cycle cryo-refrigerator. All the spectra were computer fitted and the chemical isomer shift data are quoted relative to metallic iron at room temperature.

3. Results and discussion

3.1. Synthesis results

The X-ray powder diffraction data (Fig. 2) showed evidence for successful fluorination with the fluorinated phases showing increasing cell volume with increasing level of PVDF employed (Table 1, Fig. 3). The parent material and the 1:1 fluorinated phase were both black in color, similar to the samples observed by Tsujimoto et al. [22] for fluorination with PTFE. In contrast, the colors of the 1:2 and 1:3 samples were red/brown, consistent with complete reduction to Fe^{3+} for the latter two samples. In the case of the 1:1 ratio sample, the cell volume increased by 7%, with the main effect being an increase in the *c* parameter from 20.16 to 21.43 Å. Rietveld refinement using X-ray powder diffraction data indicated complete filling of the normal anion sites, and hence a composition, $Sr_3Fe_2O_{5+x}F_{2-x}$ (see Section 3.2). The ^{57}Fe

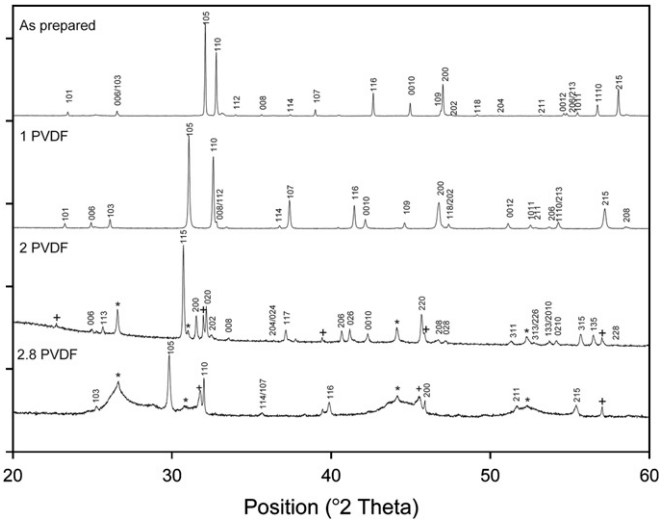

Fig. 2. X-ray diffraction patterns for $Sr_3Fe_2O_{7-x}$ as prepared, and after fluorination with 1, 2 and 2.8 mol equivalent of PVDF (*=SrF_2 phase and +=$SrFe(O/F)_3$ impurity phases).

Table 1
Cell parameters for $Sr_3Fe_2O_{7-x}$ and fluorinated phases.

System	Composition	*a*	*b*	*c*	Equivalent cell volume[a]
$Sr_3Fe_2O_{7-x}$	$Sr_3Fe_2O_{6.68(5)}$	3.86543 (2)	3.86543 (2)	20.1633 (1)	301.271 (4)
$Sr_3Fe_2O_{7-x}$:1PVDF	$Sr_3Fe_2O_{5.28(4)}F_{1.72(4)}$	3.88379 (4)	3.88379 (4)	21.4284 (2)	323.223 (8)
$Sr_3Fe_2O_{7-x}$:2PVDF	$Sr_3Fe_2O_4F_4$	5.6615 (1)	5.5540 (1)	21.3249 (6)	335.27 (4)
$Sr_3Fe_2O_{7-x}$:2.8PVDF	$Sr_3Fe_2O_3F_6$	3.9837 (2)	3.9837 (2)	22.717 (2)	360.53 (3)

[a] For the 2PVDF sample, the cell volume has been divided by 2 to allow for direct comparison between samples

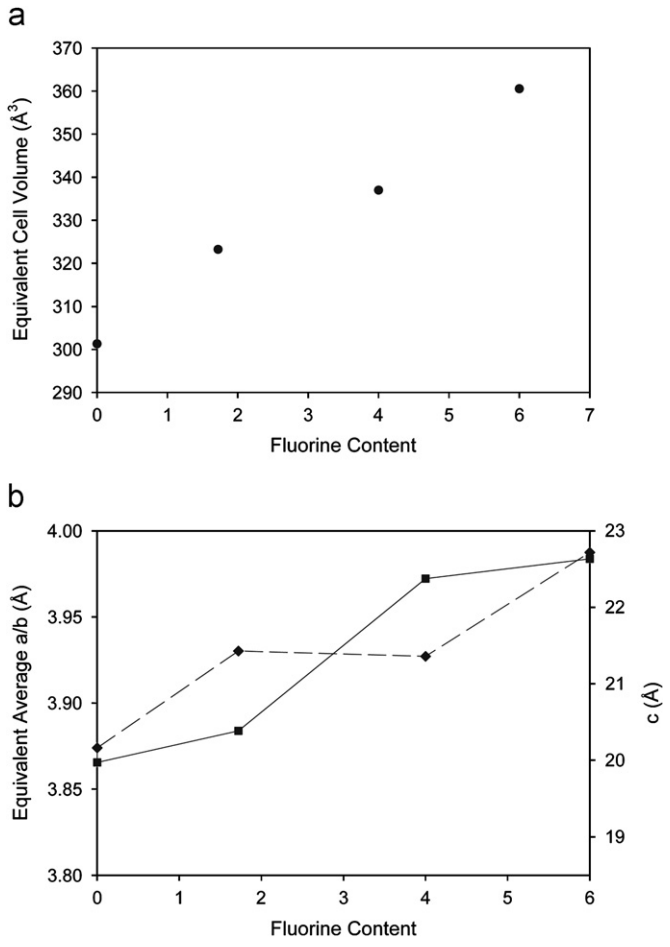

Fig. 3. (a) Variation of equivalent cell volume and (b) variation in cell lengths (full line: *a*/*b*; broken line: *c*) with F content for fluorinated $Sr_3Fe_2O_{7-x}$ samples. For the $Sr_3Fe_2O_4F_4$ sample, the average *a*, *b* axis length has been divided by $\sqrt{2}$ to allow direct comparison between all the samples.

Mössbauer data (see Section 3.3) suggested that the iron had not been completely reduced to Fe^{3+}; from the level of Fe^{4+} the composition was deduced as $Sr_3Fe_2O_{5.28}F_{1.72}$. The results are similar to the results of Tsujimoto et al. [22], where an expansion along *c* to 21.35 Å, and a composition of $Sr_3Fe_2O_{5.44}F_{1.56}$ were reported. The slightly larger expansion in cell parameters in the present case is consistent with a slightly higher fluorine content. While the study by Tsujimoto et al. of fluorination with PTFE reported no additional higher fluorine-content phases, in this work we have shown that utilizing PVDF as the fluorinating agent allows further fluorination, leading to even higher fluorine-containing phases. These additional studies have shown that on increasing the amount of PVDF employed to 2 mol, there is a further large expansion in unit cell volume, with the cell volume being 11% larger than that of the parent phase. In addition, the X-ray powder diffraction data showed evidence for peak splitting arising from a change to a lower symmetry orthorhombic cell. Somewhat surprisingly there is a small decrease in *c* compared to the 1:1 phase, with a large increase in *a*, *b* (Fig. 3b). As for the 1:1 composition, Rietveld refinement using X-ray powder diffraction data indicated complete filling of the normal anion sites but in the case of this 1:2 phase there was also evidence for partial filling of the interstitial sites (see Section 3.2). Given the ^{57}Fe Mössbauer data, which indicated that all the iron was present as Fe^{3+} (see Section 3.3), the composition was determined to be $Sr_3Fe_2O_4F_4$ with half the interstitial sites filled. For this sample, there was evidence for partial decomposition to give SrF_2 and $SrFeO_2F$ impurities. This can be understood from the high thermal stability of SrF_2 which helps to drive the decomposition reaction:

$$Sr_3Fe_2O_4F_4 \rightarrow SrF_2 + 2SrFeO_2F \quad (1)$$

Heating this sample to higher temperatures ($>600\ ^\circ C$) led to complete decomposition of the phase, showing that this fluorinated phase is metastable in line with earlier work on simple perovskite systems [6–10].

For the sample prepared with the highest amount of PVDF the X-ray powder diffraction data showed almost complete decomposition to SrF_2 and Fe_2O_3. By reducing the PVDF content to a ratio 1:2.8, a better quality sample could be obtained, although there were still large impurities (SrF_2, Fe_2O_3 and $SrFeO_2F$). In this case the X-ray powder diffraction data showed that for the fluorinated Ruddlesden Popper phase there was a large increase in *c*, and a small increase in *a*,*b*, with an overall expansion of $\approx 20\%$ compared to the parent oxide. Given the iron oxidation state of Fe^{3+} from the ^{57}Fe Mössbauer spectroscopy data (see later), the composition is believed to be close to $Sr_3Fe_2O_3F_6$ which can then readily decompose to SrF_2 and Fe_2O_3 according to the following equation:

$$Sr_3Fe_2O_3F_6 \rightarrow 3SrF_2 + Fe_2O_3 \quad (2)$$

The presence of some $SrFeO_2F$ impurity probably stems from the fact that the ratio employed was less than 1:3.

3.2. Structural refinements

X-ray powder diffraction data were used to provide a preliminary structural characterization of the fluorinated phases. Further more detailed structural refinements using neutron diffraction data are required to elucidate details of any small anion displacements as well as details of the magnetic structure.

The X-ray powder diffraction results indicated that for the 1:1 $Sr_3Fe_2O_{7-x}$:PVDF phase complete filling of the normal anion sites was achieved, similar to the results observed by Tsujimoto et al. [22] for fluorination with PTFE. Attempts to allow occupation of interstitial sites in the refinement indicated zero occupancy of these sites, and in conjunction with the Mössbauer results (Section 3.3) a composition of $Sr_3Fe_2O_{5.28}F_{1.72}$ was determined. In order to aid convergence, the atomic displacement parameters for all the anion sites were constrained as equal. The final structural parameters and selected bond distances are given in

Table 2
Structural parameters for $Sr_3Fe_2O_{5.28(4)}F_{1.72(4)}$ ($Sr_3Fe_2O_{7-x}$:1PVDF) from Rietveld refinement of X-ray diffraction data.

Atom	*x*	*y*	*Z*	100 Uiso/Å^2	Occupancy
Sr1	0	0	0.5	1.58 (6)	1
Sr2	0	0	0.32294 (4)	1.05 (5)	1
Fe1	0	0	0.08788 (8)	0.74 (5)	1
O1	0	0	0	2.45 (9)	1
O2/F2	0	0	0.2072 (3)	2.45 (9)	1
O3	0	0.5	0.0979 (2)	2.45 (9)	1

Space group *I*4/*mmm*, a=3.88379(4) Å, c=21.4284(2) Å, χ^2=2.850, Rwp=2.73%.

Table 3
Selected interatomic distances for $Sr_3Fe_2O_{5.28(4)}F_{1.72(4)}$ ($Sr_3Fe_2O_{7-x}$:1PVDF).

Bond	Bond length (Å)
Sr1–O1	2.74625(2) × 4
Sr1–O3	2.8579(33) × 8
Sr2–O2/F2	2.480(6) × 1
	2.8213(13) × 4
Sr2–O3	2.579(3) × 4
Fe1–O1	1.8831(17) × 1
Fe1–O2/F2	2.557(6) × 1
Fe1–O3	1.9536(5) × 4

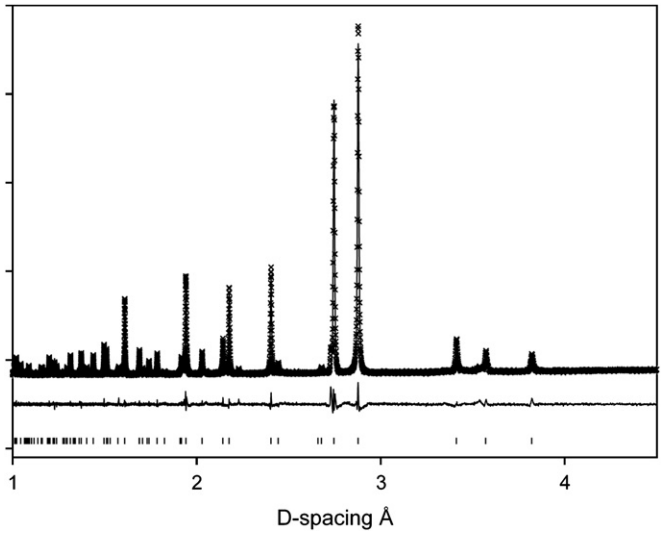

Fig. 4. Observed, calculated and difference XRD profiles for $Sr_3Fe_2O_{5.28(4)}F_{1.72(4)}$ ($Sr_3Fe_2O_{7-x}$:1PVDF).

Tables 2 and 3, with the X-ray powder diffraction profiles shown in Fig. 4. The final structural model shows that the expansion in cell parameters along the *c* direction is related to an expansion in the Fe–O2/F2 bond, which is similar to the situation observed previously for $Sr_3Fe_2O_6F_{0.87}$ and $Sr_3Fe_2O_{5.44}F_{1.56}$ prepared via fluorination with F_2 gas and PTFE, respectively [21,22]. In line with this earlier work, it was initially presumed that fluorine preferentially occupies this anion site (O2/F2) within the rock salt layers. Compared to $Sr_3Fe_2O_6F_{0.87}$, the expansion in this Fe–O2/F2 bond is much greater leading to a greater expansion along *c*, while it is similar to that observed for $Sr_3Fe_2O_{5.44}F_{1.56}$ [21,22]. These results are consistent with the much higher fluorine content in the present study and the study by Tsujimoto et al., which means that this site has approximately double the occupancy of fluorine, compared to $Sr_3Fe_2O_6F_{0.87}$. The high atomic displacement parameters for the anion sites are most likely related to disorder from the presence of mixed anion sites as noted previously for $Sr_3Fe_2O_6F_{0.87}$ [21], which may result in off-site displacements. In order to confirm the above assignment of the F position, bond valence sum (BVS) calculations were performed. With the F located in the O2 site (as described above), the calculated BVS was 3.17 (in good agreement with the expected Fe oxidation state determined from the Mössbauer results (Section 3.3) of 3.14). Placing F into the O1 or O3 sites led to lower BVS values (e.g. 3.02 for F distributed over the O1 and O2 sites, 2.98 for F in the O3 site).

For the 1:2 $Sr_3Fe_2O_{7-x}$:PVDF phase, the X-ray powder diffraction data indicated an orthorhombic cell, with space group F222 providing a good fit to the data. In this system, all the normal anion sites are filled as for the 1:1 system ($Sr_3Fe_2O_{5.28}F_{1.72}$), but there is also occupancy of half the available interstitial sites in an ordered fashion in the *ab* plane leading to a composition $Sr_3Fe_2O_4F_4$. As above, the atomic displacement parameters of the anion sites were constrained as equal to ensure convergence. The final structural parameters and selected bond distances are given in Tables 4 and 5, with the X-ray powder diffraction profiles being shown in Fig. 5 and a structural model in Fig. 6. As noted earlier, somewhat surprisingly there is a small decrease in *c* compared to that in $Sr_3Fe_2O_{5.28}F_{1.72}$ with a large increase in *a*, *b*. The structural data provide evidence for the origin of these changes showing that, compared to the structure of $Sr_3Fe_2O_{5.28}F_{1.72}$, there is a decrease in the Fe-apical anion (rock salt layer) distance, which counterbalances the expected expansion along *c* due to the partial filling of the interstitial sites. As a result, the main expansion is in the *ab* plane and the structural data suggest an ordered occupancy of half the interstitial anion sites in this plane. The driving force for the ordering is most likely

Table 4
Structural parameters for $Sr_3Fe_2O_4F_4$ ($Sr_3Fe_2O_{7-x}$:2PVDF) from Rietveld refinement of X-ray diffraction data.

Atom	*x*	*y*	*z*	100*Uiso	Occupancy
Sr1	0	0	0.5	1.1 (2)	1
Sr2	0	0	0.3177 (2)	1.3 (2)	1
Fe1	0	0	0.0877 (4)	2.0 (2)	1
O1	0.25	0.25	0.103 (2)	5.2 (3)	1
O2	0.25	0.25	0.911 (2)	5.2 (3)	1
F1	0	0	0	5.2 (3)	1
F2	0	0	0.189 (1)	5.2 (3)	1
F3	0.25	0.25	0.75	5.2 (3)	1

Space group *F*222, a=5.6615(1) Å, b=5.5540(1) Å, c=21.3249(6) Å, χ^2=1.698, Rwp=3.76%.

Table 5
Selected interatomic distances for $Sr_3Fe_2O_4F_4$ ($Sr_3Fe_2O_{7-x}$:2PVDF).

Bond	Bond length (Å)
Sr1–F1	2.77697(6) × 2
	2.83076(7) × 2
Sr1–O1	2.954(32) × 4
Sr1–O2	2.738(32) × 4
Sr2–F2	2.752(22) × 1
	2.7802(11) × 2
	2.8339(11) × 2
Sr2–O1	2.611(29) × 2
Sr2–O2	2.816(33) × 2
Sr2–F3	2.4523(22) × 2
Fe1–F1	1.870(8) × 1
Fe1–F2	2.152(2) × 1
Fe1–O1	2.008(7) × 2
Fe1–O2	1.9828(4) × 2

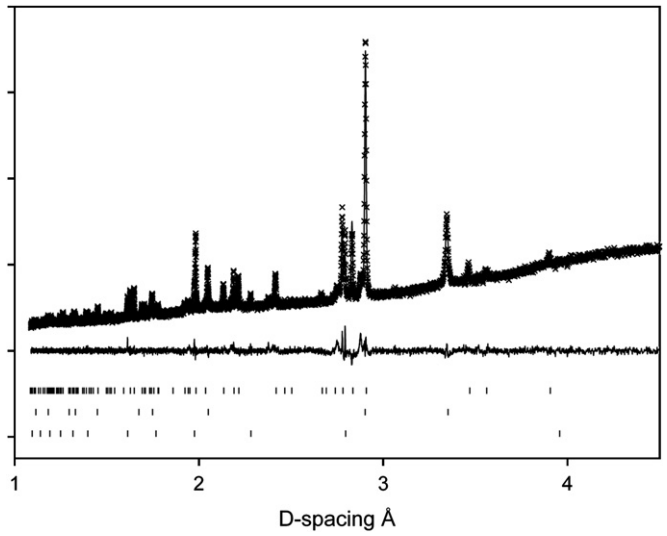

Fig. 5. Observed, calculated and difference XRD profiles for $Sr_3Fe_2O_4F_4$ ($Sr_3Fe_2O_{7-x}$: 2PVDF) (upper tick marks: $Sr_3Fe_2O_4F_4$, lower tick marks: $SrFeO_2F$, middle tick marks: SrF_2. Phase fraction ratios relative to $Sr_3Fe_2O_4F_4$ (1.0)=0.420(10) SrF_2, 0.425(15) $SrFeO_2F$).

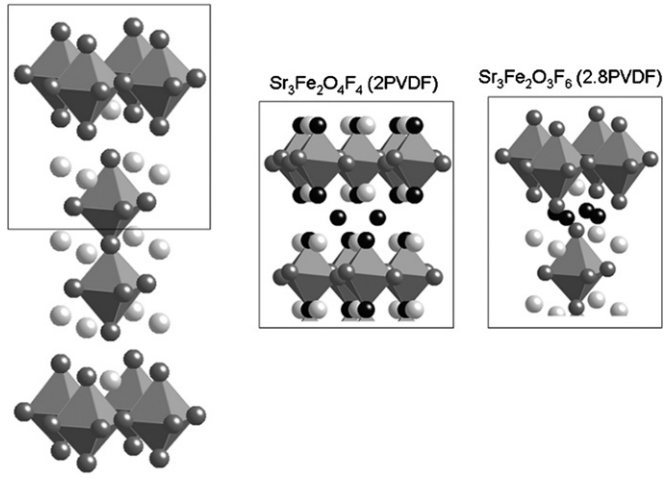

Fig. 6. Structures of fluorinated $Sr_3Fe_2O_{7-x}$ showing the changes on increasing F content; $Sr_3Fe_2O_{5.28(4)}F_{1.72(4)}$ has an ideal $n=2$ Ruddlesden Popper phase with complete filling of the normal anion sites, and no occupancy of the interstitial sites; in $Sr_3Fe_2O_4F_4$, half the interstitial sites are additionally filled; in $Sr_3Fe_2O_3F_6$, the interstitial sites are now completely filled.

to ensure maximum separation of the anions within the interstitial sites. Although the O and F cannot be distinguished by X-ray powder diffraction, it is presumed that in this phase fluorine occupies the interstitial sites and all the apical sites (as noted in Table 4), leaving the oxygen to occupy the equatorial sites in the FeO_2 layers. In order to provide evidence in support of this O/F distribution, BVS calculations were performed, which gave a value of 2.97 for the above assignment, in good agreement with the presence of only Fe^{3+}. In contrast, other O/F distributions led to lower BVS values, e.g. 2.75 for F in the equatorial sites (O1, O2), 2.86 for a random distribution of F.

The structural data also show high values of the atomic displacement parameters for the anion sites, which suggests significant local displacements, most likely associated with the effect of the presence of these interstitial anions on adjacent anions. In order to make further detailed conclusions, neutron diffraction studies are required to provide a more accurate description of the anion sites, as well as to elucidate the magnetic structure.

For the 1:2.8 $Sr_3Fe_2O_{7-x}$:PVDF sample, no structure refinement was performed due to the large impurities present in this sample. Instead only the cell parameters for the fluorinated phase were determined. However, as noted above it is presumed that this phase has a composition close to $Sr_3Fe_2O_3F_6$, which would correspond to complete filling of both the normal anion and interstitial sites (Fig. 6), the additional filling of the interstitial sites contributing to the cell expansion along the *c* axis. The composition is in agreement with the decomposition impurity products (SrF_2 and Fe_2O_3; Eq. (2)) observed by X-ray powder diffraction. In terms of occupancy of the anion sites, it is presumed that F occupies all the interstitial sites, the apical sites, and ¼ of the equatorial sites within the Fe layers.

3.3. Mössbauer spectroscopy data

3.3.1. $Sr_3Fe_2O_{7-x}$:1PVDF ($Sr_3Fe_2O_{5.28}F_{1.72}$)

The ^{57}Fe Mössbauer spectra are collected in Fig. 7 and the parameters given in Table 6. The initial fitting of these spectra was directed towards the characterization of the oxidation state of iron especially in the light of previous evidence for the disproportionation of Fe^{4+} into Fe^{5+} and Fe^{3+} in $Sr_3Fe_2O_6F_{0.87}$ [21] and $Sr_3Fe_2O_{5.44}F_{1.56}$ [22]. The classical method of deducing the oxidation state of iron from a Mössbauer spectrum is via the chemical isomer shift. The comparison of the recorded chemical

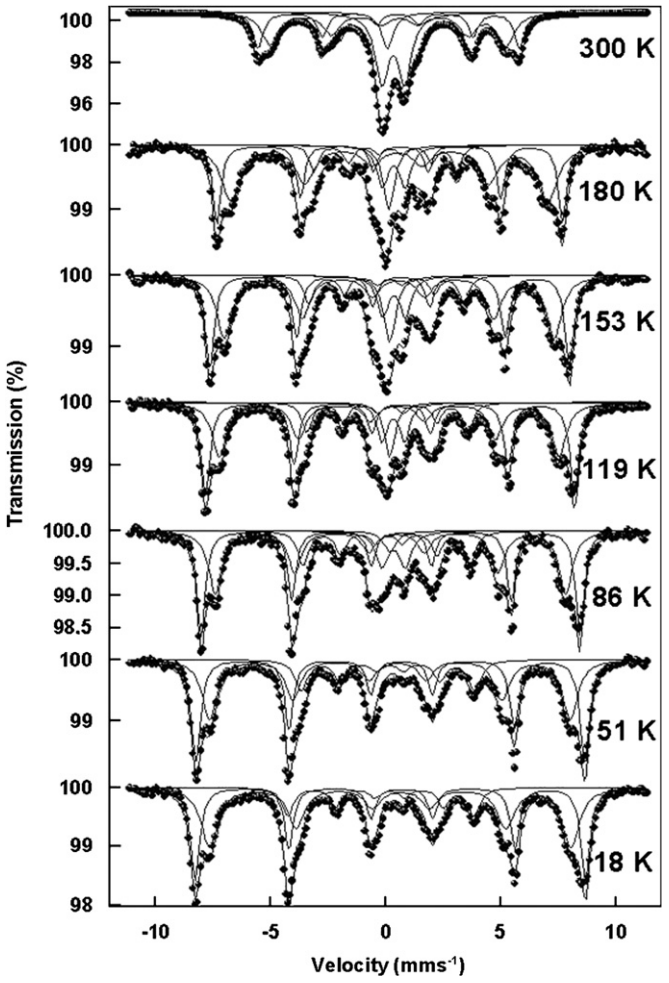

Fig. 7. ^{57}Fe Mössbauer spectra recorded from $Sr_3Fe_2O_{5.28(4)}F_{1.72(4)}$ ($Sr_3Fe_2O_{7-x}$: 1PVDF).

Table 6
^{57}Fe Mössbauer parameters recorded from fluorinated $Sr_3Fe_2O_{7-x}$.

Material	Temperature of measurement	Assignment	$\delta \pm 0.02$ (mm s^{-1})	Δ or $e^2Qq/2 \pm 0.05$ (mm s^{-1})	$H \pm 5$ (T)	Area ± 5%
$Sr_3Fe_2O_{5.28}F_{1.72}$	300	Fe^{4+}	0.08			7
		Fe^{3+}	0.34	1.00		30
		Fe^{3+}	0.34	−0.38	35.2	25
		Fe^{3+}	0.37	−0.5	21.8	38
	180	Fe^{4+}	0.15			8
		Fe^{3+}	0.36	1.00		10
		Fe^{3+}	0.34	−0.32	42.7	45
		Fe^{3+}	0.42	−0.48	46.6	28
		Fe^{4+}	0.11	−0.20	19.2	10
	153	Fe^{4+}	0.18			8
		Fe^{3+}	0.38	1.00		9
		Fe^{3+}	0.36	−0.38	44.4	39
		Fe^{3+}	0.43	−0.48	48.5	33
		Fe^{4+}	0.11	−0.12	20.9	11
	119	Fe^{4+}	0.18			6
		Fe^{3+}	0.34	1.00		9
		Fe^{3+}	0.34	−0.34	45.8	38
		Fe^{3+}	0.44	−0.48	49.7	35
		Fe^{4+}	0.15	−0.12	21.7	13
	86	Fe^{4+}	0.18			3
		Fe^{3+}	0.37	1.00		9
		Fe^{3+}	0.35	−0.25	47.2	34
		Fe^{3+}	0.46	−0.48	51.0	39
		Fe^{4+}	0.15	−0.06	22.4	15
	56	Fe^{3+}	0.36	−0.32	48.6	40
		Fe^{3+}	0.46	−0.48	52.4	43
		Fe^{4+}	0.15	−0.08	23.3	18
	18	Fe^{3+}	0.37	−0.32	48.9	45
		Fe^{3+}	0.46	−0.48	52.7	39
		Fe^{4+}	0.14	−0.10	23.4	16
$Sr_3Fe_2O_4F_4$	300	Fe^{3+}	0.34	0.89		6
		Fe^{3+}	0.36	−0.12	53.5	2
		Fe^{3+}	0.45	−0.03	50.6	1
		Fe^{3+}	0.39	−0.30	39.2	91
	180	Fe^{3+}	0.43	0.81		6
		Fe^{3+}	0.46	−0.32	48.1	94
	100	Fe^{3+}	0.5	−0.32	52.5	100
	80	Fe^{3+}	0.5	−0.25	52.8	100
	20	Fe^{3+}	0.5	−0.35	53.5	100
$Sr_3Fe_2O_3F_6$	300	Fe^{3+}	0.35	0.98		84
		Fe^{3+}	0.37[a]	0.26	51.4	4
		Fe^{3+}	0.4	−0.60	51.2	3
		Fe^{3+}	0.34	0.12	25.5	9
	180	Fe^{3+}	0.43	0.98		68
		Fe^{3+}	0.40[a]	−0.18	54.6	5
		Fe^{3+}	0.40	0.76	54.7	3
		Fe^{3+}	0.45	−0.46	42.4	19
		Fe^{3+}	0.32	1.13	41.7	5
	148	Fe^{3+}	0.43	1.03		39
		Fe^{3+}	0.45[a]	−0.22	54.7	5
		Fe^{3+}	0.45	0.36	55.0	3
		Fe^{3+}	0.45	−0.46	46.6	16
		Fe^{3+}	0.45	1.16	45.3	6
		Fe^{3+}	0.45	−0.74	45.4	2
		Fe^{3+}	0.45	−0.92	32.9	2
		Fe^{3+}	0.24	−0.20	18.7	28
	118	Fe^{3+}	0.41	1.00		10
		Fe^{3+}	0.45[a]	−0.22	55.0	4
		Fe^{3+}	0.45	0.36	55.0	3
		Fe^{3+}	0.47	−0.52	50.3	17
		Fe^{3+}	0.45	0.9	49.2	8
		Fe^{3+}	0.45	−0.05	45.4	7
		Fe^{3+}	0.45	−0.16	39.6	10
		Fe^{3+}	0.39	0.03	26.2	41
	78	Fe^{3+}	0.45[a]	−0.22	55.0	4
		Fe^{3+}	0.45	0.36	55.0	3
		Fe^{3+}	0.47	−0.52	50.3	16
		Fe^{3+}	0.47	0.52	49.2	13
		Fe^{3+}	0.47	−0.02	45.4	22
		Fe^{3+}	0.47	−0.03	39.6	14
		Fe^{3+}	0.40	0.20	26.2	28
	51	Fe^{3+}	0.45[a]	−0.22	55.0	5

Table 6 (*continued*)

Material	Temperature of measurement	Assignment	$\delta \pm 0.02$ (mm s^{-1})	Δ or $e^2Qq/2 \pm 0.05$ (mm s^{-1})	$H \pm 5$ (T)	Area $\pm$ 5%
		Fe^{3+}	0.45	0.36	55.0	3
		Fe^{3+}	0.47	−0.50	51.0	17
		Fe^{3+}	0.48	0.26	49.8	13
		Fe^{3+}	0.48	−0.01	46.6	31
		Fe^{3+}	0.41	−0.08	41.9	23
		Fe^{3+}	0.40	0.1	26.0	8
	23	Fe^{3+}	−0.48	−0.22	55.0	5
		Fe^{3+}	0.48	0.36	55.0	3
		Fe^{3+}	0.48	−0.56	51.2	16
		Fe^{3+}	0.52	0.13	50.0	27
		Fe^{3+}	0.46	−0.01	47.0	32
		Fe^{3+}	0.38	−0.10	42.7	16

[a] $=\alpha$-Fe_2O_3.

isomer shifts with values from related components in the literature enables the assignment of the oxidation states of iron in the material under investigation. There is a large body of data in the literature which associates chemical isomer shifts around 0.35 mm s^{-1} with Fe^{3+} (for example [24,25]), around 0.05 mm s^{-1} with Fe^{4+} (see for example [25,26]), and below −0.05 mm s^{-1} even at low temperatures with Fe^{5+} (see for example [18,19,21]). The Mössbauer spectrum recorded at 300 K from $Sr_3Fe_2O_{5.28}F_{1.72}$ showed the presence of a singlet with a chemical isomer shift 0.08 mm s^{-1} which, from the discussion above, we associate with paramagnetic Fe^{4+} together with a paramagnetic doublet with chemical isomer shift of 0.34 mm s^{-1} characteristic of Fe^{3+}. The two magnetic sextet components visible in the spectrum recorded at 300 K ($\delta = ca.$ 0.34–0.37 mm s^{-1}) are typical of the presence of Fe^{3+} and demonstrate that, in contrast to the $Sr_3Fe_2O_{7-x}$ and $Sr_3Fe_2O_6F_{0.87}$ systems [21], some Fe^{3+} is amenable to magnetic ordering at this temperature. The parameters of the sextets are very similar to those shown by Fe^{3+} in the $n=1$ Ruddlesden Popper compound Sr_2FeO_3F, which has the K_2NiF_4 structure [27], which is consistent with the structural model indicating the presence of fluorine in the apical sites leading to FeO_5F octahedra as in Sr_2FeO_3F. At 180 K a well-defined magnetic sextet component ($\delta = 0.11$ mm s^{-1}) with a smaller magnetic hyperfine field (19.2 T) appeared which we associate with the paramagnetic Fe^{4+} component observed at 300 K. The intensity of this sextet increased at the expense of the intensity of the paramagnetic Fe^{4+} singlet as the temperature decreased to *ca.* 56 K and, between 86 and 18 K, showed a magnetic hyperfine field of *ca.* 23 T which is not dissimilar from that observed in other Fe^{4+}-containing materials [26]. The Fe^{4+} content of the material was difficult to estimate because of the complexity of the spectra but, given the intensities of the Fe^{4+} component in the totally magnetically ordered spectra recorded at lower temperature where the differences in recoil-free fractions among the different species are minimized, we would suggest that an Fe^{4+} content of *ca.*14 ± 2% might be an appropriate approximation: from this, the composition $Sr_3Fe_2O_{5.28(4)}F_{1.72(4)}$ was evaluated. Given the increase in lattice parameters upon fluorination (see above) which exceeded those recorded recently for the material $Sr_3Fe_2O_{5.44}F_{1.56}$ [22] our results are consistent with the higher fluorine content in the present study. The presence of Fe^{4+} and Fe^{3+}, rather than Fe^{3+} and Fe^{5+} as in $Sr_3Fe_2O_6F_{0.87}$ produced by fluorination of $Sr_3Fe_2O_6$ by gaseous fluorine [21] and in $Sr_3Fe_2O_{5.44}F_{1.56}$ [22], would suggest that high levels of fluorine are required to suppress the disproportionation of Fe^{4+} in these systems.

The paramagnetic Fe^{3+} absorption accounts for *ca.* 30% of the spectral area at 300 K and decreases in intensity until 56 K when all the Fe^{3+} is magnetically ordered. The quadrupole interactions for the two Fe^{3+} sextets are quite large and would indicate a distortion of the anion or electronic array around Fe^{3+} and reflects the presence of both oxygen and more electronegative fluorine. Assuming that the fluorine is located on the apical sites then magnetic Fe^{3+}–O^{2-}–Fe^{3+}superexchange interactions within planes which manifest themselves as sextet components in the Mössbauer spectrum even at 300 K is reasonable.

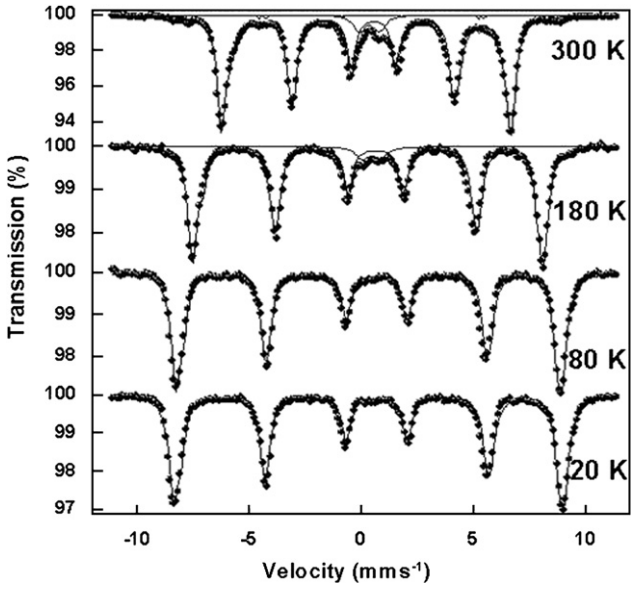

Fig. 8. ^{57}Fe Mössbauer spectra recorded from $Sr_3Fe_2O_4F_4$ ($Sr_3Fe_2O_{7-x}$:2PVDF).

3.3.2. $Sr_3Fe_2O_{7-x}$:2PVDF ($Sr_3Fe_2O_4F_4$)

All the Mossbauer spectra were amenable to fitting to a number of components with chemical isomer shifts characteristic of Fe^{3+} (Fig. 8, Table 6).The Mössbauer spectrum recorded at 300 K from this compound showed the presence of an intense, asymmetric broad magnetic component, indicative of the presence of a distribution of hyperfine magnetic fields, two additional weak sextets with much larger hyperfine magnetic fields, and a paramagnetic doublet. The two weak sextets have parameters which are compatible with the presence of $SrFeO_2F$ [7] and therefore endorse the identification by X-ray powder diffraction of this impurity phase. The doublet persists at 180 K and the main magnetic component, although still showing an asymmetric

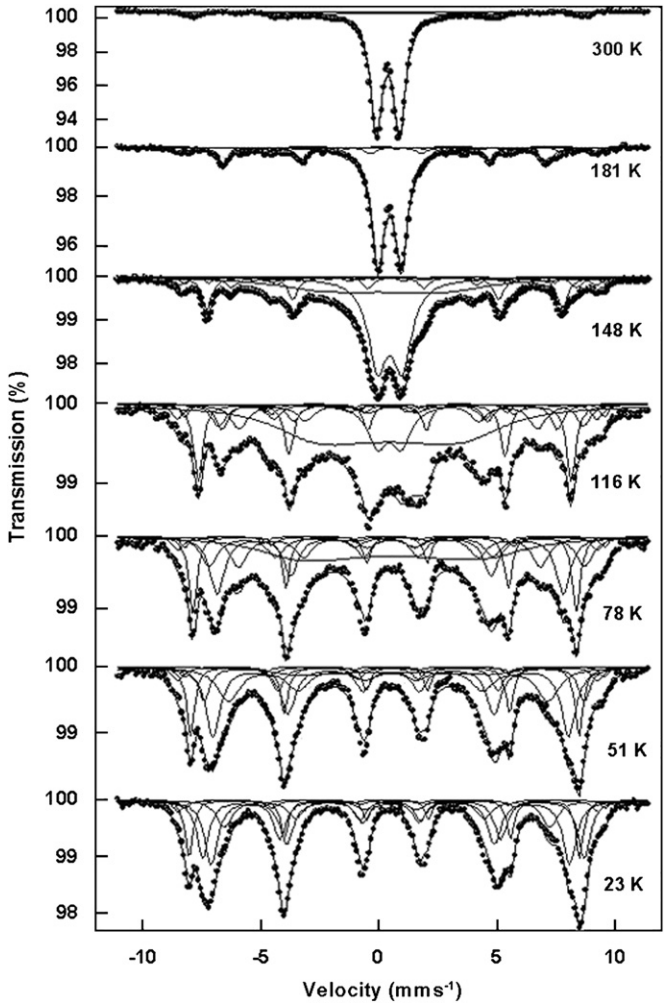

Fig. 9. ^{57}Fe Mössbauer spectra recorded from $Sr_3Fe_2O_3F_6$ ($Sr_3Fe_2O_{7-x}$:2.8PVDF).

shape, present narrower lines than at 300 K. Below 180 K the two small sextets are completely masked by the asymmetric magnetic component and they were not taken into account in the fit of the spectra. The main component is characterized by relatively large values of $e^2Qq/2$, both factors (the asymmetry of the spectral lines and the large quadrupole shift values) being indicative of a distorted electronic or anionic environment around Fe^{3+} and a reflection of the more electronegative fluorine in some of the anion sites and different local distortions around the Fe^{3+} ions.

3.3.3. $Sr_3Fe_2O_{7-x}$:2.8PVDF ($Sr_3Fe_2O_3F_6$)

The Mössbauer spectra (Fig. 9, Table 6) showed only the presence of Fe^{3+}, most of which is paramagnetic at 300 K. The spectrum at 300 K also showed a broad magnetic component with low hyperfine field and two small, although well defined, sextets characterized by quite large magnetic fields which can be associated with the presence of $SrFeO_2F$[7] and the α-Fe_2O_3 impurity suggested by X-ray powder diffraction. The behavior of the Mössbauer spectra recorded with decreasing temperature is complex and is characterized by the coexistence of the paramagnetic doublet and different sextet components over a large range of temperatures (from 300 to 78 K). This behavior is consistent with the occurrence of structural disorder reflecting dissimilar configurations around the Fe^{3+} ions such that they magnetically order at different temperatures. These different configurations might be related to the presence of fluorine in equatorial sites such that the Fe^{3+}–O^2 –Fe^{3+} superexchange pathways in this sample are inhibited by Fe^{3+}–F–Fe^{3+} interactions.

4. Conclusions

Low temperature fluorination of the Ruddlesden Popper phase $Sr_3Fe_2O_{7-x}$ with PVDF has been achieved to produce three new oxide fluorides, assigned as $Sr_3Fe_2O_{5+x}F_{2-x}$ ($x \approx 0.28$), $Sr_3Fe_2O_4F_4$ and $Sr_3Fe_2O_3F_6$. As the fluorine content is increased the normal anion sites are firstly filled while, for higher fluorine contents, progressive filling of the interstitial anion sites occurs. Particularly for these higher fluorine contents, the phases are unstable to decomposition due to the high thermodynamic stability of the decomposition product SrF_2. The Mössbauer data indicate that the magnetic interactions in these phases are complex and reflect the heterogeneity of local oxygen and fluorine compositions around the iron ions and their influence on superexchange interactions. Overall, the results show the versatility of low temperature fluorination of perovskite-related oxides with PVDF for the production of new oxide fluorides with high fluorine contents.

Acknowledgments

We would like to express thanks to EPSRC for funding (studentship for CAH). The Bruker D8 diffractometer and Netzsch STA 449 F1 Jupiter Thermal Analyser used in this research was obtained through the Science City Advanced Materials project: Creating and Characterising Next generation Advanced Materials project, with support from Advantage West Midlands (AWM) and part funded by the European Regional Development Fund (ERDF). Financial support from the Spanish Ministry of Science and Technology through project MAT2009-14578-C03-01 is also acknowledged.

References

[1] M. Sturza, S. Daviero-Minaud, H. Kabbour, O. Gardoll, O. Mentré, Chem. Mater. 22 (2010) 6726.
[2] M. Sturza, H. Kabbour, S. Daviero-Minaud, D. Filimonov, K. Pokholok, N. Tiercelin, O. Mentré, J. Am. Chem. Soc. 28 (2011) 10901.
[3] M. Al Mamouri, P.P. Edwards, C. Greaves, M. Slaski, Nature 369 (1994) 382.
[4] P.R. Slater, J.P. Hodges, M.G. Francesconi, P.P. Edwards, C. Greaves, I. Gameson, M. Slaski, Physica C 253 (1995) 16.
[5] E.E. McCabe, C. Greaves, J. Fluorine Chem. 128 (2007) 448.
[6] F.J. Berry, X. Ren, R. Heap, P.R. Slater, M.F. Thomas, Solid State Commun. 134 (2005) 621.
[7] F.J. Berry, R. Heap, Ö. Helgason, E.A. Moore, S. Shim, P.R. Slater, M.F. Thomas, J. Phys. Condens. Matter 20 (2008) 215207.
[8] R. Heap, P.R. Slater, F.J. Berry, Ö. Helgason, A.J. Wright, Solid State Commun. 141 (2007) 476.
[9] O. Clemens, R. Haberkorn, P.R. Slater, H.P. Beck, Solid State Sci. 12 (2010) 1455.
[10] F.J. Berry, F.C. Coomer, C. Hancock, Ö. Helgason, E.A. Moore, P.R. Slater, A.J. Wright, M.F. Thomas, J. Solid State Chem. 184 (2011) 1361.
[11] P.R. Slater, J. Fluorine Chem. 117 (2002) 43.
[12] T. Baikie, E.L. Dixon, J.F. Rooms, N.A. Young, M.G. Francesconi, Chem. Commun. (2003) 1580.
[13] T. Sivakumar, J.B. Wiley, Mater. Res. Bull. 44 (2009) 74.
[14] Y. Kobayashi, M. Tian, M. Eguchi, T.E. Mollouk, J. Am. Chem. Soc. 131 (2009) 9849.
[15] M. Abbate, L. Mogni, F. Prado, A. Caneiro, Phys. Rev. B 71 (2005) 195113.
[16] F. Prado, A. Manthiram, J. Solid State Chem. 158 (2001) 307.
[17] K. Kuzushita, S. Morimoto, S. Nasu, S. Nakamura, J. Phys. Soc. Jpn. 69 (2000) 2767.
[18] P. Adler, J. Solid State Chem. 130 (1997) 129.
[19] S.E. Dann, M.T. Weller, D.B. Currie, M.F. Thomas, A.D. Alrawwas, J. Mater. Chem. 3 (1993) 1231.
[20] S.E. Dann, M.T. Weller, D.B. Currie, J. Solid State Chem. 97 (1992) 179.
[21] G.S. Case, A.L. Hector, W. Levason, R.L. Needs, M.F. Thomas, M.T. Weller, J. Mater. Chem. 9 (1999) 2821.

[22] Y. Tsujimoto, K. Yamaura, N. Hayashi, K. Kodama, N. Igawa, Y. Matsuhita, Y. Katsuya, Y. Shirako, M. Akaogi, E. Takayama-Muromachi, Chem. Mater. (2011). doi:10.1021/cm201075g.
[23] A.C. Larson and R.B. Von Dreele Los Alamos National Laboratory, Report No LA-UR-96-748 (1987).
[24] D.P.E. Dickson, F.J.Berry (Eds.), Mössbauer Spectroscopy.Cambridge University Press, Cambridge, 1986.
[25] F. Menil, J. Phys. Chem. Solids. 46 (1985) 763.
[26] P. Adler, A. Lebon, V. Damljanovic, C. Ulrich, C. Bernhard, A.V. Boris, A. Maljuk, C.T. Lin, B. Kiemer, Phys. Rev B 73 (2006) 94451.
[27] A.L. Hector, J.A. Hutchings, R.L. Needs, M.F. Thomas, M.T. Weller, J. Mater. Chem. 11 (2001) 527.